Uptake and Cellular Distribution of Nucleolar Targeting Peptides (NrTPs) in Different Cell Types

Margarida Rodrigues,[1] David Andreu,[2] Nuno C. Santos[1]
[1]*Instituto de Medicina Molecular, Faculdade de Medicina, Universidade de Lisboa, Lisbon, Portugal*
[2]*Department of Experimental and Health Sciences, Pompeu Fabra University, Barcelona Biomedical Research Park, Barcelona, Spain*

Received 4 November 2014; revised 5 January 2015; accepted 11 January 2015
Published online 23 January 2015 in Wiley Online Library (wileyonlinelibrary.com). DOI 10.1002/bip.22610

ABSTRACT:

Nucleolar targeting peptides (NrTPs) are a family of cell penetrating peptides (CPPs) derived from crotamine, a rattlesnake venom toxin. They were named NrTPs for their remarkable nucleolus-homing properties and have been studied for their potential as drug delivery vehicles. Live cell microscopy experiments were conducted to monitor NrTP uptake and distribution in different cell types, including primary cells (PBMCs and erythrocytes) and different immortalized cell lines (HeLa, BHK21, BV-173, and MOLT-4). Uptake dependence on cell type (primary vs. immortalized, suspension vs. adherent, cancer vs. healthy cells), peptide concentration and cell viability were evaluated. To gain further insight on the internalization mechanism, uptake kinetics was also monitored. Results showed the uptake and distribution pattern as strongly dependent on peptide sequence, peptide concentration and membrane constituents. Under similar conditions, NrTP6 is more internalized than NrTP1, NrTP2 and NrTP5. Additionally, while internalization of NrTP7 and NrTP8 may cause cytotoxicity, NrTP6 is noncytotoxic. Higher peptide concentrations can be correlated to nucleolar targeting, although even at low concentrations a residual number of cells reveal positive nucleolar labeling. NrTPs were successfully internalized into all cell types tested except erythrocytes. © 2015 Wiley Periodicals, Inc. Biopolymers (Pept Sci) 104: 101–109, 2015.

Keywords: *cell penetrating peptides; NrTP; uptake kinetics; microscopy*

Correspondence to: Nuno C. Santos, Instituto de Medicina Molecular, Faculdade de Medicina, Universidade de Lisboa, Lisbon, Portugal; e-mail:nsantos@fm.ul.pt
Contract grant sponsor: Fundação para a Ciência e a Tecnologia—Ministério da Educação e Ciência (FCT-MEC, Portugal), including M.R. PhD fellowship
Contract grant number: SFRH/BD/37432/2007
Contract grant sponsor: Spanish Ministry of Economy and Competitiveness (MINECO)
Contract grant number: SAF2011–24899
Contract grant sponsor: Generalitat de Catalunya
Contract grant number: 2009 SGR 492
Contract grant sponsor: FP7-PEOPLE IRSES project MEMPEPACROSS (European Union)

This article was originally published online as an accepted preprint. The "Published Online" date corresponds to the preprint version. You can request a copy of any preprints from the past two calendar years by emailing the Biopolymers editorial office at biopolymers@wiley.com.

INTRODUCTION

Cell penetrating peptides (CPPs) are short, usually less than 30-residue sequences that can cross cell membranes, either alone or as vehicles for the delivery of specific molecular cargos. The first protein to be recognized as a CPP, in what was termed a "collateral" discovery, was HIV-1 Tat.[1] Compared with other drug delivery strategies, CPPs show key advantages such as reduced immunogenicity, wide range of application (given their small size) and ease of production. Currently, most authors agree that there is no universal mechanism for CPP internalization. Regarding individual CPPs, opinions also tend to diverge, as often there is experimental evidence for both endocytic and nonendocytic internalization pathways for the same peptide.[2] These discrepancies can sometimes be correlated with differences in the methodological parameters used in each

study. Importantly, direct translocation and endocytosis can coexist in time and cellular environment for the same CPP.[3,4] Together, the CPP itself, its local concentration, the cellular model and the cargo determine the nature of the uptake mechanism(s) or which one prevails.[4] Despite their considerable mechanistic differences, endocytosis and direct translocation are likely to share relevant membrane features as part of the internalization route. One of such candidates are cell surface heparan sulfate proteoglycans (HSPG), as their involvement has been periodically suggested and indirectly demonstrated.[5,6]

NrTPs (nucleolar targeting peptides) are derived from crotamine, a 42-amino acid residue toxin from the venom of the South-American rattlesnake *Crotalus durissus terrificus*.[7] NrTP1 (YKQCHKKGGKKGSG) resulted from the splicing of crotamine N- (residues 1–9) and C- (38–42) terminal sections.[8] Several NrTP1 analogues were also studied (Table I), including a 6-aminohexanoic acid spacer moiety (NrTP2), the all-D enantiomer (NrTP5), the Cys→Ser replacement (NrTP6), and NrTP6 with full Lys→Arg (NrTP7) or Tyr→Trp replacement (NrTP8). Initial studies supported the original design considerations, i.e., the importance of charged regions at N- and C-termini for cellular internalization.[8] In that study, a remarkable ability of the peptides to co-localize with nucleoli was observed, leading to the nucleolar targeting peptide denomination. Later on, NrTP interaction with membrane model systems and its bearing on activity was studied, showing extensive interaction with both zwitterionic and negatively charged membranes.[9] Also, the NrTP ability to ferry a large enzyme (β-galactosidase) cargo into cells, maintaining its catalytic activity, was experimentally demonstrated.[10]

In order to better characterize the cellular internalization of NrTPs, peptide uptake was tested in different cell types, and followed by live cell microscopy. Experiments were conducted using both primary (PBMCs and erythrocytes) and immortalized (HeLa, BHK21, BV-173, and MOLT-4 cell lines) mammalian cells. These cell types were chosen to maximize the different aspects to be compared: sample origin (primary vs. immortalized cell line), pathophysiology (healthy vs. tumor), tissue (fibroblasts vs. blood cells), and growth (adherent vs. suspension). PBMCs (peripheral blood mononuclear cells), blood cells with a single round nucleus, include lymphocytes (T, B, and NK cells), monocytes and dendritic cells, all of them immune system cells with specific roles in fighting infection. Erythrocytes, the most abundant of blood cells, involved in O_2-delivery to all body tissues, have membranes with the essential properties of deformability and stability, especially important for traversing the capillary network. HeLa and BHK21 (baby hamster kidney) cells are both fibroblastic cells, the most common cells in the connective tissue of animals, responsible for the synthesis of collagen and the extracellular matrix, and with a critical role in wound healing. BV-173 and MOLT-4 are human lymphoblastic cells derived from B-cell precursor cells of chronic myeloid leukemia and T-lymphoblastic leukemia patients, respectively.

Table I Amino Acid Sequences for Crotamine-Derived Peptides

NrTP	Sequence
1	YKQCHKKGGKKGSG
2	YKQCHKKGGKKGSG
5	ykqchkkGGkkGsG
6	YKQSHKKGGKKGSG
7	YRQSHRRGGRRGSG
8	WKQSHKKGGKKGSG

NrTP2 contains a molecular spacer, 6-aminohexanoic acid (Ahx), NrTP5 is the D-enantiomer of NrTP1, NrTP6 contains a Ser residue instead of the original Cys, in NrTP7 all Lys were replaced by Arg and in NrTP8 Tyr was replaced by Trp.

MATERIALS AND METHODS

Peptides

The solid phase synthesis of N-terminal rhodamine B (RhB)-labeled peptides NrTP1 (YKQCHKKGGKKGSG), NrTP2 (with a 6-aminohexanoic acid spacer between GG and KK), NrTP5 (enantiomer of NrTP1), NrTP6 (Cys replaced by Ser), NrTP7 (all 5 Lys changed to Arg), and NrTP8 (Tyr replaced by Trp) have been described earlier.[8,9] $Tat_{48–60}$ (GRKKRRQRRRPPQ-amide) was similarly synthesized by solid phase methods. All peptides were purified to >95% homogeneity by analytical HPLC and further analyzed by MALDI-TOF mass spectrometry, revealing the expected molecular masses and confirming purity. Sequences are shown in Table I.

Microscopes

Imaging was conducted on a Zeiss LSM 510 META confocal point-scanning microscope (Jena, Germany), with a large size incubator for temperature control set at 37°C. The lasers used were diode 405–30 (405 nm; 50 mW), diode-pumped solid-state (DPSS; 561 nm; 15 mW) and HeNe633 (633 nm; 5 mW), together with a 63× (NA 1.4, oil) Zeiss Plan-Apochromat objective. Phase contrast images were acquired using the 561 nm laser and a photomultiplier for transmitted light. A motorized wide-field fluorescence microscope Zeiss Axiovert 200M equipped with a small stage incubator for temperature control and CO_2 supply and a sensitive cooled CCD camera (Roper Scientific Coolsnap HQ CCD) was also used in some experiments. Images were acquired with a 63× oil Plan-Apochromat objective, using the red filter (FS15), excitation 540 to 552 nm and emission >590 nm. Images obtained using either microscope were processed using ImageJ (rsbweb.nih.gov/ij/).

Cell Maintenance and Isolation

All immortalized cell lines were cultured in T-flasks (75 cm^2) at 37°C and 5% CO_2. HeLa and BHK21 cells (both adherent) were

maintained in Dulbecco's modified eagle medium (DMEM) supplemented with 10% (v/v) FBS, 100 U/mL penicillin, and 100 μg/mL streptomycin. BV-173 and MOLT-4 (suspension cells) were cultured in RPMI-1640 supplemented with 10% (v/v) FBS, 2 mM L-glutamine, 1 mM sodium pyruvate, 100 U/mL penicillin, and 100 μg/mL. Erythrocytes and PBMCs were isolated from human blood samples collected from healthy donors, with their previous written informed consent, following a protocol established with the Portuguese Blood Institute (IPS—Lisbon), approved by the joint Ethics Committee of the Faculty of Medicine of the University of Lisbon and Santa Maria Hospital. PBMCs were isolated by density gradient using Ficoll-Paque Plus (GE Healthcare, Little Chalfont, UK) following a protocol described elsewhere.[11] After the last washing step, PBMCs were resuspended in PBS supplemented with 10% (v/v) FBS, counted and kept at 4°C. For erythrocytes isolation, blood samples were centrifuged at 1200 *g* during 10 min to remove plasma and buffy-coat. Erythrocytes were washed three times with PBS pH 7.4 and a 10% hematocrit suspension was prepared.

Confocal Microscopy

For the internalization experiments, 1.2×10^4 of HeLa or BHK21 cells were seeded 24 h to 48 h prior the experiment in eight-well Ibidi-treated plates (μ-slide eight-well; Ibidi, Munich, Germany). The culture medium was aspirated 2 h before the beginning of the experiment, cells washed with PBS, and the culture medium replaced by DMEM/F-12 (DMEM without phenol red), without supplements, and cells returned to the incubator to stabilize. Regarding BV-173 and MOLT-4 cells, immediately before the experiment, cells were washed in PBS, centrifuged twice at 100 *g*, counted and resuspended in PBS. Cells were then plated in the eight-well Ibidi-treated plates at a density of 2×10^6 cells/mL. Experiments using PBMCs and erythrocytes started 30 min to 1 h after cell isolation. Incubation with NrTPs was conducted in 1.5 mL microcentrifuge tubes at 4×10^6 PBMCs/mL or at a final hematocrit of 0.0875% (approximately 10.5×10^6 erythrocytes/mL). Before imaging, 200 μL of PBMC or erythrocyte suspension were transferred to eight-well Ibidi-treated plates. RhB-NrTPs concentrations were tested between 5 and 30 μM. Peptides were either let to incubate with cells for 2 h prior imaging or added to the cells already under the microscope, at 37°C (and 5% CO_2 for immortalized cells). Besides peptides' RhB, 2.5 μg/mL Hoechst 33342 (350/461 nm, Invitrogen/Molecular Probes, Eugene, OR) was used for nuclear staining, and 0.25 μM TO-PRO3 (642/661 nm, Invitrogen/Molecular Probes) as a viability dye. These probes were incubated with the cells at 37°C and 5% CO_2 for 20 to 30 min, 10 to 15 min, and 15 to 20 min, respectively.

Uptake Kinetics Followed by Wide-Field Microscopy

BHK21 cells were used to follow the kinetics of NrTPs uptake. 6×10^4 cells were seeded 24 to 48 h prior the experiment onto ibiTreat µ-dishes (Ibidi), and maintained in DMEM supplemented with 10% (v/v) FBS, 10 U/mL penicillin and 100 μg/mL streptomycin, at 37°C, and in the presence of 5% CO_2. Cells were washed with PBS 2 to 3 h before experiment, and the culture medium replaced by DMEM/F12 without supplements. Before imaging, ibiTreat µ-dishes were adjusted and stabilized in the stage incubator (set for 37°C and 5% CO_2) using modeling clay. Software was programmed to take images (*z*-stacks; five focal planes or optical section) every 5 min in a 3×3 matrix-like arrangement (nine areas), during 2 h (~1100 images/peptide/experiment). Each of these areas was checked and the best focal plane for the first area to be imaged was set as the reference plane ($z = 0$). Optical sectioning was added to prevent loss of correct focal plane during the experiment. Finally, the peptide was added and image acquisition started. Data analysis was performed using ImageJ. Briefly, the first processing consisted in the selection of the best slice from the *z*-stack (for each of the nine areas, for each peptide and experiment). For each peptide, nine time-lapse series were obtained, each one made of 26 frames. Following, we selected individual cells using the ROI (region of interest) manager tool from ImageJ, as indicated in Figure 6A. Then, the intensity values for each region and time point were calculated and plotted as in Figures 6B–6D.

RESULTS AND DISCUSSION

Internalization of NrTPs into different cell types

HeLa Cells. Incubations were performed with rhodamine B (RhB)-labeled NrTPs and $Tat_{48–60}$ (positive control) both at 5 μM (data not shown) and 15 μM. Both concentrations yielded successful cellular translocation; however, as expected, the fluorescence signal is higher at 15 μM, and the differences between the different peptides become more evident. Results for cells incubated with 15 μM of peptide are displayed in Figure 1. A nuclear stain (Hoechst 33342) and a viability probe (TO-PRO3, a membrane-impermeable dye that binds double-stranded DNA when membrane integrity is compromised) were also used. Results confirmed the ability of NrTPs to be internalized into HeLa cells and the existence of different staining patterns: cells with solely cytoplasmic staining (partly endocytic, partly free), or with both cytoplasmic (nonendocytic) and nuclear (especially nucleolar) staining; in all cells, nuclear staining was lower than cytoplasmic or nucleolar staining. Thus, for NrTP1, NrTP2, NrTP5, and NrTP6 at 15 μM, virtually all cells presented an exclusively cytoplasmic staining (partly endocytic, partly free), without positive labeling for TO-PRO3. On the other hand, for NrTP7, NrTP8, and $Tat_{48–60}$, the fraction of cells with nuclear (mainly nucleolar) staining increased, also revealing positive TO-PRO3 staining. $Tat_{48–60}$ was by far the most cytotoxic peptide, not only exhibiting the strongest TO-PRO3 labeling but also significant overall morphologic changes (chromatin condensation and extensive cellular shrinkage), as evidenced by the transmitted light images. In general, a correlation could be found between peptide nucleolar labeling and positive TO-PRO3 staining.

MOLT-4 Cells. All NrTPs were successfully internalized into MOLT-4 cells (Figure 2), with peptide uptake following a similar trend than for HeLa cells. NrTP6 was the best performing peptide, showing high levels of internalization without apparent viability loss (even at 30 μM). Once again, nucle(ol)ar

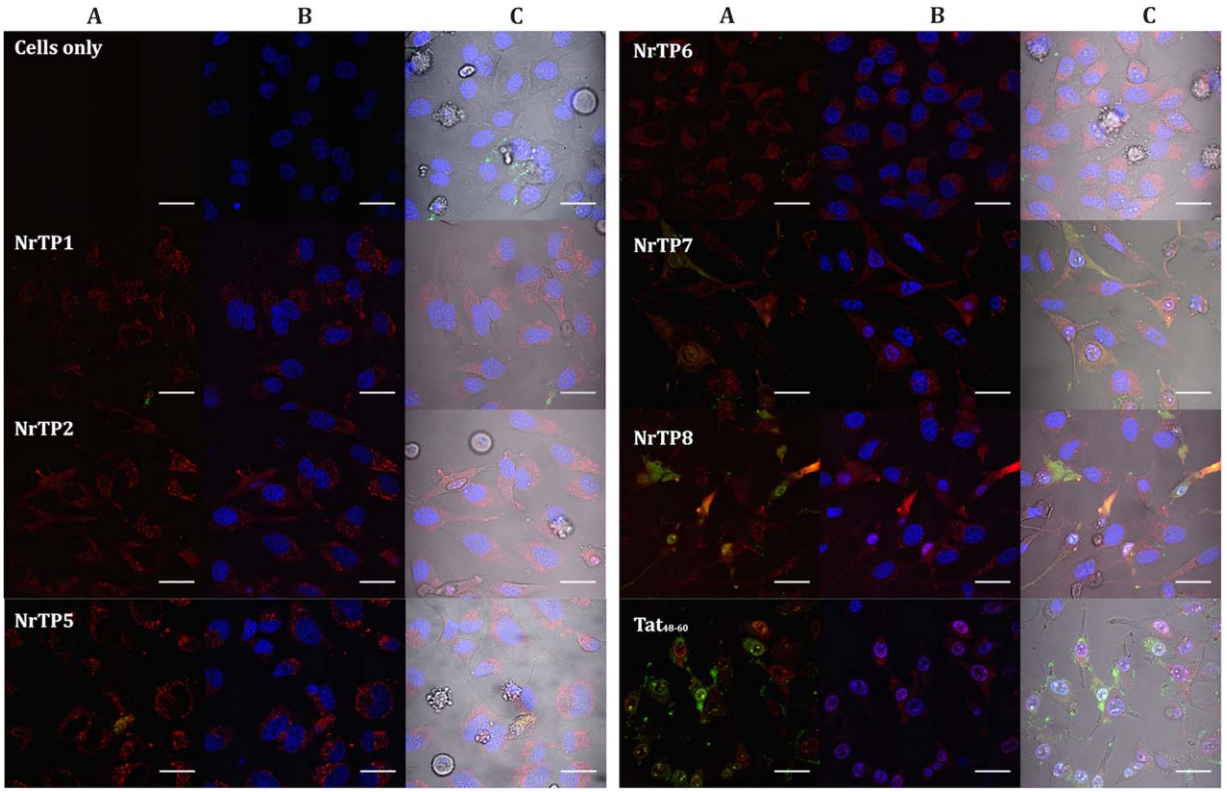

FIGURE 1 HeLa cells incubated with RhB-NrTPs(or $Tat_{48–60}$) 15 μM at 37°C and 5% CO_2. Each horizontal sequence of three images corresponds to a different NrTP. (A) Co-localization of peptide fluorescence (RhB) and cell viability (TO-PRO3); (B) co-localization of peptide fluorescence (RhB) and nuclei staining (Hoechst 33342); and (C) co-localization of transmitted light with the previous images. Hoechst 33342 (blue), RhB (red) and TO-PRO3 (green) are detected upon excitation with the 405 nm, 561 nm and 633 nm lasers, respectively. Scale bars = 30 μm.

localization of peptide coincided with TO-PRO3 staining, with NrTP7, NrTP8, and the $Tat_{48–60}$ control showing higher percentages of TO-PRO3 positive cells. In addition, NrTP7 and $Tat_{48–60}$ presented morphologic alterations and indications of apoptosis and chromatin condensation (smaller and brighter nucleus).

Taken together, the results hitherto observed for both HeLa and MOLT-4 cells agree with previous reports on this CPP family.[9,11] The similar behavior of NrTP1 and NrTP5 is consistent with the absence of a chiral receptor for peptide internalization. For NrTP6, with just a Cys→Ser replacement relative to NrTP1, an important increase in peptide uptake was noted (clearer for MOLT-4 cells). It would appear that the Cys residue, which was shown to remain in free thiol form under the conditions of incubation,[9,11] interferes to some degree with one or more internalization steps. NrTP7 is comparable to $Tat_{48–60}$ in terms of cytotoxicity. Both peptides are rich in Arg residues, which are known to increase both peptide internalization and toxicity.[6,12] The Tyr→Trp replacement in NrTP8 also caused a significant increase in cytotoxicity, which is unlikely to be related to the minor increase in hydrophobicity. The influence of one or more Trp residues in the cytotoxicity of membrane-active peptides has been extensively studied, given their role within the membrane and the prevalence of Trp close to the lipid-water interface on protein transmembrane regions. In CPPs, the most frequent position for a Trp is close to one of the termini.[13] Moreover, if the Trp is adjacent to a cationic residue when the peptide is in α-helical conformation, its cytotoxicity increases.[14] In the present case, the Trp was added to the N-terminal domain, which corresponds to an α-helix in the crotamine structure, next to a Lys residue. Therefore, it can be suggested that NrTP8 overall lower CPP efficiency and increased cytotoxicity compared with NrTP6 can be explained by a stronger interaction with the cell membrane, different from those of other NrTPs.

Erythrocytes. Figure 3 shows that erythrocyte incubation with NrTP6 or NrTP7 gave no sign of translocation (no positive signal for RhB). Erythrocytes did, however, show membrane alterations and an apparent decrease in cell number, especially

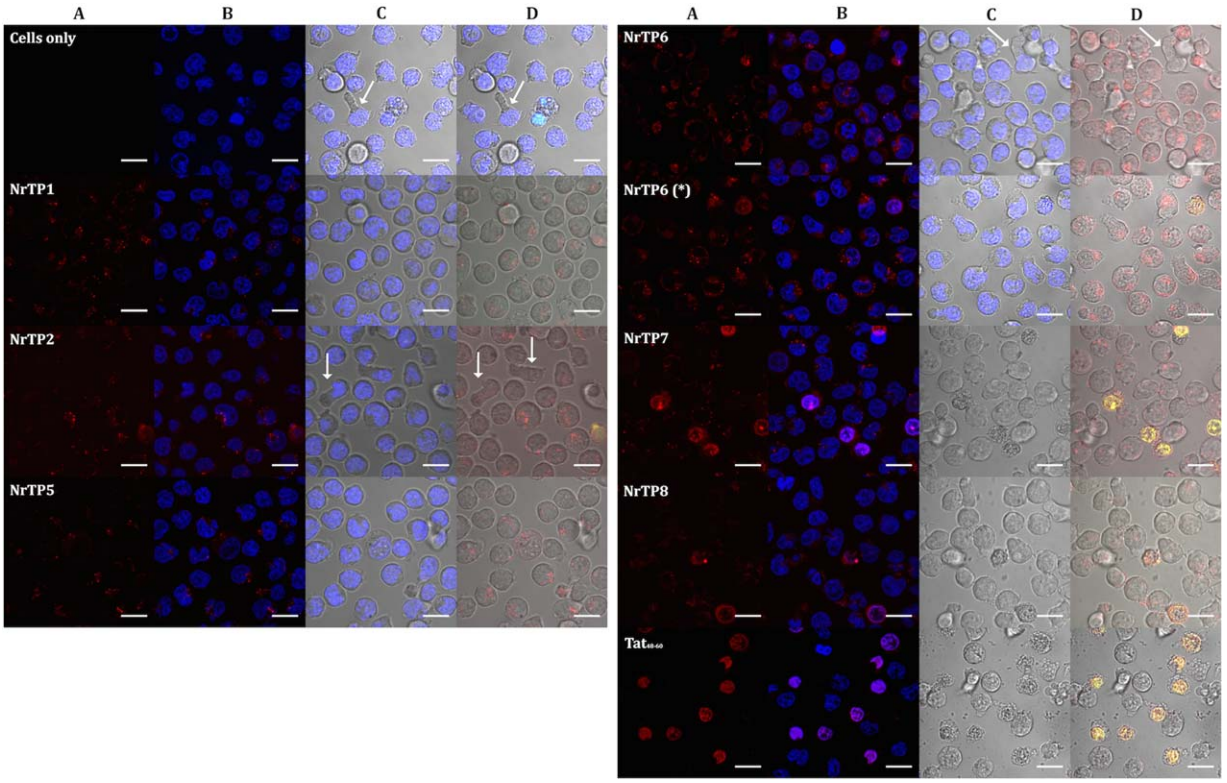

FIGURE 2 MOLT-4 (human acute T-lymphoblastic leukemia) cells incubated with RhB-NrTPs(or $Tat_{48–60}$) 15 μM (except for (*) where 30 μM were used), at 37°C and 5% CO_2. Each horizontal sequence of four images corresponds to a different NrTP. From left to right: (A) peptide's fluorescence (RhB); (B) co-localization of RhB and nuclei staining (Hoechst 33342); (C) co-localization of transmitted light with Hoechst 33342; and (D) co-localization of RhB with the viability probe (TO-PRO3) and transmitted light. Hoechst 33342 (blue), RhB (red), and TO-PRO3 (green) are detected upon excitation with the 405 nm, 561 nm, and 633 nm lasers, respectively. White arrows indicate moving cells. Scale bars = 15 μm.

in the presence of NrTP7. The spiculated surface shown by erythrocyte upon NrTP7 exposure indicates that the CPP induced echinocyte formation, a reversible type of erythrocyte morphology. These experiments highlighted two important aspects: first, none of the peptides was internalized into erythrocytes (contrary to what was observed for the other cells tested); and secondly, when compared with NrTP7, NrTP6 showed a much milder effect on cell viability and general membrane alterations (as for the other cell types). Further support to these results comes from a detailed observation of the

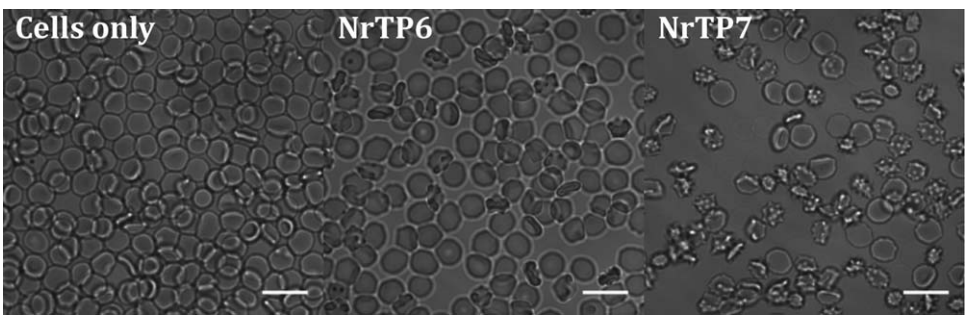

FIGURE 3 Erythrocytes incubated with RhB-NrTP6 or RhB-NrTP7 15 μM, at 37°C. Co-localization of peptide's fluorescence (RhB) with transmitted light. Scale bars = 15 μm.

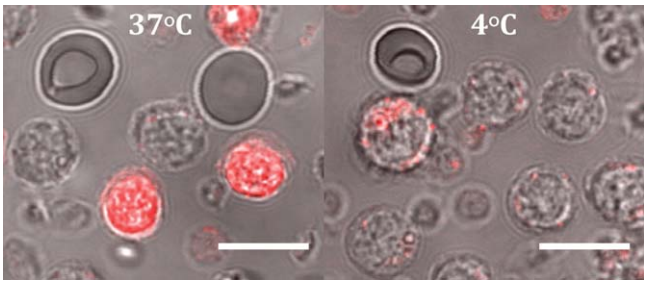

FIGURE 4 Presence of erythrocytes in a PBMCs suspension incubated with RhB-NrTP1 15 μM, at 4 or 37°C. Co-localization of peptide's fluorescence (RhB) with transmitted light. Scale bars = 10 μm.

images from PBMCs incubation with NrTPs (both at 4 and 37°C). Contrary to PBMCs, erythrocytes do not show signs of peptide uptake (Figure 4).

It can be hypothesized that this absence of translocation is related to membrane differences between erythrocytes and other cells tested, as well as to differences in general cell morphophysiology, such as the absence of nucleus and subcellular organelles. The lipids present in the erythrocyte membrane are fairly similar to those of other mammalian cells, although specific percentages may vary significantly (e.g., cholesterol is much more abundant than in other cell membranes).[15,16] It is commonly accepted that mature erythrocytes lack endocytic machinery.[17,18] However, drug-induced endocytosis in erythrocytes is extensively described,[19,20] as well as the use of erythrocytes as drug carriers.[21] On those situations, erythrocyte membrane internalization is a regulated metabolic process dependent on drug concentration (high concentrations cause hemolysis), temperature (37°C) and pH (pH 7.9–8.1).[20] The overall erythrocyte membrane surface charge is negative, mainly due to the presence of sialic acid residues.[22] On the other hand, in most cells, HSPG are among the main contributors for the negative surface charge. These molecules have been extensively implicated in the internalization of CPPs.[6,23] It is believed that HSPG facilitate peptide binding to the membrane and promote internalization. NrTP6 and mostly NrTP7 have the ability to bind the membrane of erythrocytes, apparently without subsequent internalization. This coincides with the observations by Åmand et al.[6] that CPP uptake in HSPG-deficient cells is seriously impaired when compared with normal ones, though surface binding was similar.

Another significant difference between, erythrocytes and other mammalian cells, is the transmembrane potential, which is approximately −8 mV for erythrocytes and significantly more negative for other cells.[24] As NrTPs have positive net charge (+5), peptide accumulation in the erythrocyte membrane is much less favorable than for other cells with more negative transmembrane potential. Alternatively, it can be hypothesized that NrTP internalization is impaired due to the absence or limitations on endocytic pathways, as these peptides enter cells mainly by endocytosis[11] and mature erythrocytes are deficient in most of the molecules of the endocytic machinery.[20] It is also possible that pH and peptide concentration used were just not ideal to trigger drug-induced endocytosis. Finally, the absence of nucleus in erythrocytes might also be associated with the impaired CPP activity of NrTPs for these blood cells.

BHK21, BV-173, and PBMCs. We have also tested NrTP uptake by BHK21, BV-173 and PBMCs. Figure 5 displays some of the results obtained for these cells. For the sake of brevity, only one peptide per cell type is presented. NrTPs were efficiently internalized into BV-173, BHK21 and PBMCs, with a distribution pattern similar to that previously described for HeLa and MOLT-4 cells. Although NrTPs were not internalized by erythrocytes, they successfully entered PBMCs,

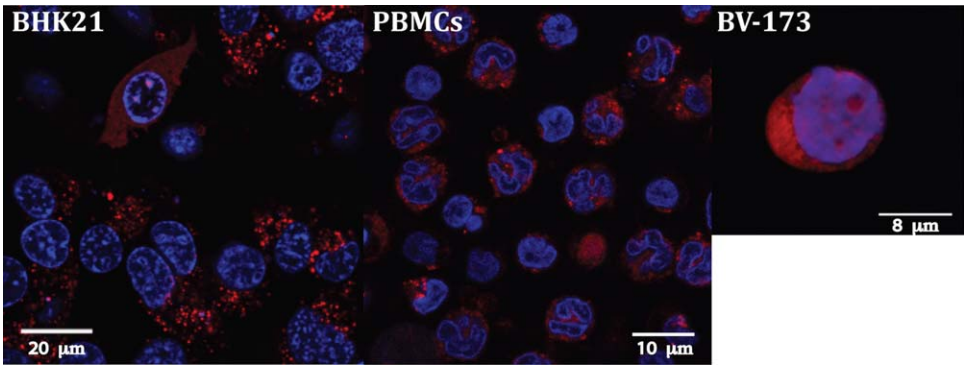

FIGURE 5 Different cell types incubated with RhB-NrTPs, at 37°C and 5% CO_2. From left to right, BHK21 cells incubated with RhB-NrTP2, PBMCs incubated with RhB-NrTP6 and BV-173 cells incubated with RhB-NrTP1. Hoechst 33342 (blue) and RhB (red) were detected upon excitation with the 405 nm and 561 nm lasers, respectively.

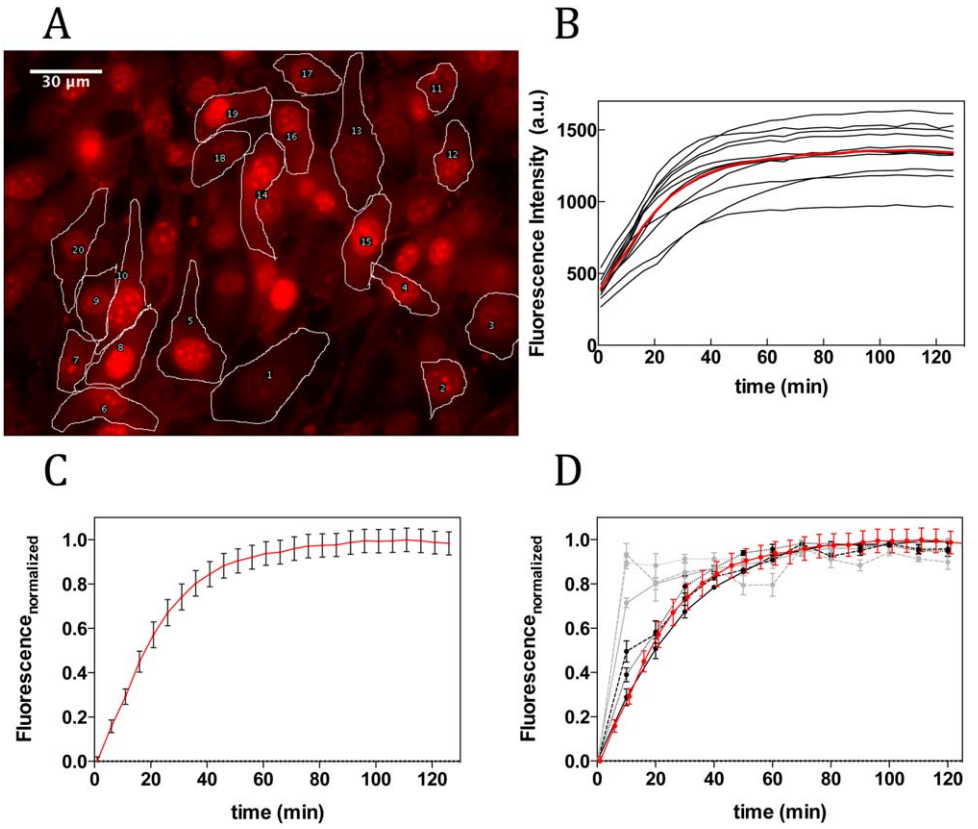

FIGURE 6 Kinetic profiles of RhB-NrTP8 uptake into BHK21 and PBMCs. (A) Representation of individual BHK21cell selection for intensity measurements. (B) Intensity profiles of cells incubated with RhB-NrTP8 30 μM at 37°C during 2 h. Each black line corresponds to the fluorescence intensity of a single cell. The red line is the average intensity from the profiles obtained. (C) Normalized values and standard error of the mean (SEM) for the red profile represented in (B). (D) Superimposition of normalized kinetic profiles obtained for RhB-NrTP8 incubated with BHK21 (red), lymphocytes (gray), or monocytes (black), together with the respective SEM (lymphocytes and monocytes results are from a previous work[11]). The multiple lines for lymphocytes and monocytes correspond to the three concentrations tested (2, 5, and 15 μM).

excluding the possibility that peptide entry would be restricted to adherent cells. Also, internalization into PBMCs and BHK21 (the two models of healthy cells) demonstrates the ability of NrTPs to penetrate both healthy and cancer cells.

Uptake Kinetics Monitored by Live Cell Microscopy

Figure 6 depicts the internalization kinetics of RhB-NrTP8, followed by live cell microscopy. Figure 6A is a representative image, with individual cells selected for intensity measurement, while the fluorescence time-courses are plotted in Figures 6B–6D. The kinetic profile can be described as a saturation-like curve, typical of first-order kinetics. In a previous study, we have evaluated the kinetics of NrTP uptake into PBMCs by flow cytometry.[11] Those results revealed significant differences in terms of uptake mechanism between lymphocytes and monocytes, the two main PBMC cell subsets. Interestingly, comparison of NrTP8 uptake into BHK21 and PBMCs[11] shows very similar profiles for BHK21 and monocytes (see Figure 6D), hence possible similarities in the uptake mechanism. As previously suggested, a strong role for endocytosis on NrTP cellular internalization is envisaged. However, direct translocation may also have its part[9], especially in the case of very low or high extracellular concentrations. Figure 7 presents selected time frames and the intensity profiles for two lines, each including the following regions: µ-dish background, cell membrane, cytosol, nucleus, and nucleoli. Intensity plots reveal preferential localization in the nucleoli, regardless of time. After 20 min incubation, nucleoli clearly show the highest fluorescence signal.

CONCLUSION

In this study, we compared the ability of NrTPs to be internalized into different cell types, including primary and

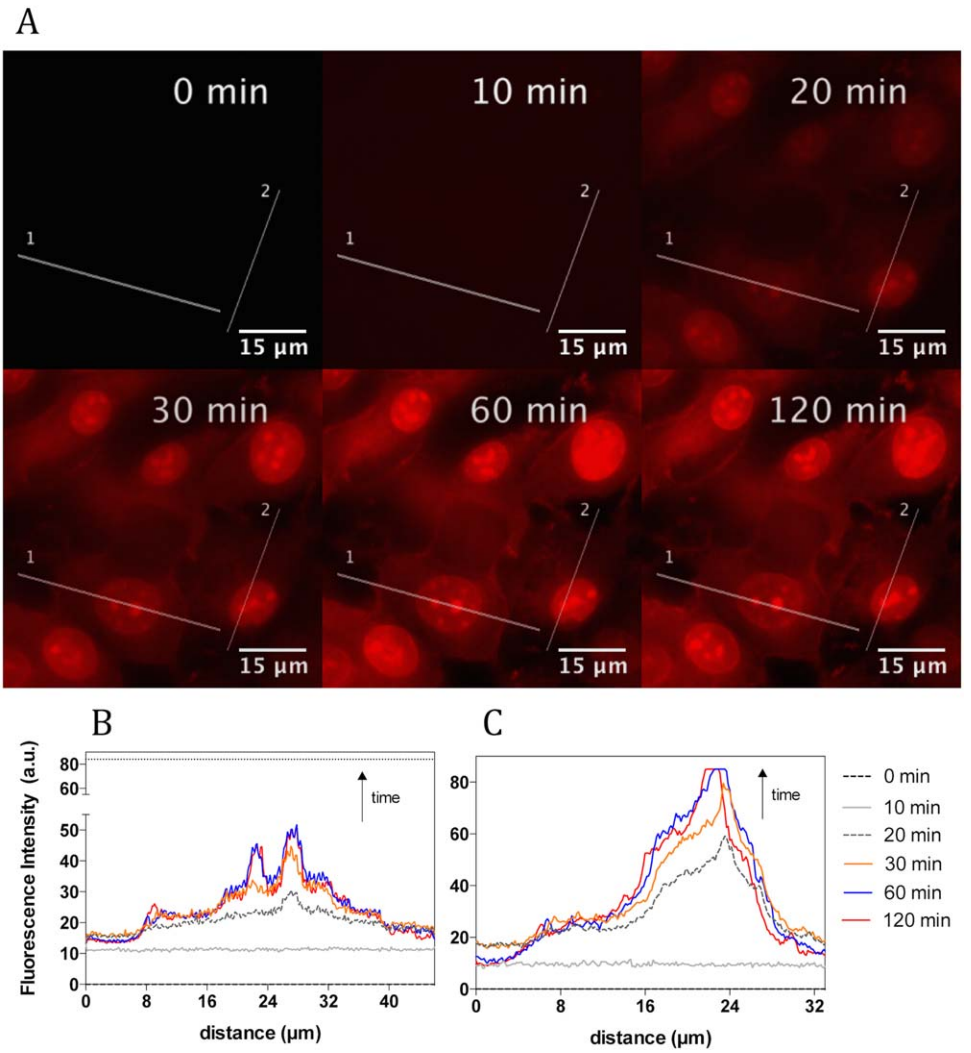

FIGURE 7 Uptake of RhB-NrTP8 into BHK21 cells. (A) Selected timeframes from time-lapse microscopy of BHK21 cells incubated with RhB-NrTP8 30 μM, during 2 h, at 37°C. (B) and (C) Plots correspond to fluorescence intensity profiles measured along the straight lines drawn in (A), 1 (B), and 2 (C), respectively, for each time point.

immortalized cells, healthy and tumor cells, as well as adherent and suspension cells. Results showed successful NrTP uptake in all cell types tested, except erythrocytes. NrTPs could be found in the cytosol, nucleus, and nucleoli of these cells. Peptide sequence and extracellular concentration influence the amount internalized and localization of the peptide. Additionally, as explained above, the labeling pattern can be correlated to some extent with cell viability, as TO-PRO3 is found in cells that display nucleolar (or nuclear) staining.

Although the present microscopy studies do not allow precise quantitative comparisons, they indicate that viability is concentration dependent. All peptides except NrTP6 (for which no signs of increasing toxicity from 5 to 30 μM were observed) revealed higher percentages of TO-PRO3-positive cells at 15 μM than at 5 μM (data not shown).

As NrTPs are not cell-specific, any possible specificity and physiological function will rely solely in the cargo. It is worth noticing that the ability of NrTPs to enter healthy primary cells without compromising cell viability is a relevant advantage, as CPPs should be harmless if one intends to use them as molecular carriers. Another important idea is that in all cell types where we tested these crotamine-derived peptides, the trend of uptake efficiency versus viability was maintained, strengthening the importance of peptide sequence.

HeLa and BHK21 cells were gently provided by Sónia Sá Santos (IMM), and BV-173 and MOLT-4 cells by Telma Lança and Julie Ribot (IMM).

REFERENCES

1. Frankel, A. D.; Frankel, A. D.; Pabo, C. O.; Pabo, C. O. Cell 1988, 55, 1189–1193.
2. Madani, F.; Lindberg, S.; Langel, U.; Futaki, S.; Gräslund, A. J Biophys 2011, 2011, 1–10.
3. Poon, G. M. K.; Gariépy, J. Biochem Soc Trans 2007, 35, 788.
4. Walrant, A.; Walrant, A.; Bechara, C.; Bechara, C.; Alves, I. D.; Alves, I. D.; Sagan, S.; Sagan, S. Nanomedicine 2012, 7, 133–143.
5. Joliot, A. H.; Joliot, A. H.; Pernelle, C.; Pernelle, C.; Deagostini-Bazin, H.; Deagostini-Bazin, H.; Prochiantz, A.; Prochiantz, A. Proc Natl Acad Sci USA 1991, 88, 1864–1868.
6. Åmand, H. L.; Rydberg, H. A.; Fornander, L. H.; Lincoln, P.; Nordén, B.; Esbjörner, E. K. Biochim Biophys Acta 2012, 1818, 2669–2678.
7. Kerkis, A.; Kerkis, I.; Rádis-Baptista, G.; Oliveira, E. B.; Vianna-Morgante, A. M.; Pereira, L. V.; Yamane, T. FASEB J 2004, 18, 1407–1409.
8. Rádis-Baptista, G.; la Torre de, B. G.; Andreu, D. J Med Chem 2008, 51, 7041–7044.
9. Rodrigues, M.; Santos, A.; la Torre, de, B. G.; Rádis-Baptista, G.; Andreu, D.; Santos, N. C. Biochim Biophys Acta 2012, 1818, 2707–2717.
10. Rodrigues, M.; la Torre, de, B. G.; Rádis-Baptista, G.; Santos, N. C.; Andreu, D. Bioconjug Chem 2011, 22, 2339–2344.
11. Rodrigues, M.; la Torre, de, B. G.; Andreu, D.; Santos, N. C. Biochim Biophys Acta 2013, 1830, 4554–4563.
12. Mitchell, D. J.; Kim, D. T.; Steinman, L.; Fathman, C. G.; Rothbard, J. B. J Pept Res 2000, 56, 318–325.
13. Jones, A. T.; Sayers, E. J. J Control Release 2012, 161, 582–591.
14. Rekdal, O.; Haug, B. E.; Kalaaji, M.; Hunter, H. N.; Lindin, I.; Israelsson, I.; Solstad, T.; Yang, N.; Brandl, M.; Mantzilas, D.; Vogel, H. J. J Biol Chem 2011, 287, 233–244.
15. Matos, P. M.; Freitas, T.; Castanho, M. A. R. B.; Santos, N. C. Biochem Biophys Res Commun 2010, 403, 270–274.
16. Leidl, K.; Liebisch, G.; Richter, D.; Schmitz, G. Biochim Biophys Acta 2008, 1781, 655–664.
17. Lopez-Estraño, C.; Bhattacharjee, S.; Harrison, T.; Haldar, K. Proc Natl Acad Sci USA 2003, 100, 12402–12407.
18. Haldar, K.; Mohandas, N. Curr Opin Hematol 2007, 14, 203–209.
19. Schrier, S. L.; Chiu, D. T.; Yee, M.; Sizer, K.; Lubin, B. J Clin Invest 1983, 72, 1698–1705.
20. Rossi, L.; Serafini, S.; Magnani, M. Erythrocyte Engineering for Drug Delivery and Targeting; Landes Bioscience: New York, 2003.
21. Muzykantov, V. R. Expert Opin Drug Deliv 2010, 7, 403–427.
22. Oliveira, S. de ; Saldanha, C. Clin Hemorheol Microcirc 2010, 44, 63–74.
23. Nakase, I.; Nakase, I.; Tadokoro, A.; Tadokoro, A.; Kawabata, N.; Kawabata, N.; Takeuchi, T.; Takeuchi, T.; Katoh, H.; Katoh, H.; Hiramoto, K.; Hiramoto, K.; Negishi, M.; Negishi, M.; Nomizu, M.; Nomizu, M.; Sugiura, Y.; Sugiura, Y.; Futaki, S.; Futaki, S. Bioconjug Chem 2007, 46, 492–501.
24. Cheng, K.; Haspel, H. C.; Vallano, M. L.; Osotimehin, B.; Sonenberg, M. J Membr Biol 1980, 56, 191–201.